Scientific Research Publishing

Computational Chemistry, 2024, 12, 57-74
https://www.scirp.org/journal/cc
ISSN Online: 2332-5984
ISSN Print: 2332-5968

S_EAr Mechanism of the Products of 1,2-Dimethoxybenzene and a Captodative Olefin: A Theoretical Approach

René Santana-García[1], Judit Aviña-Verduzco[1], Rafael Herrera-Bucio[1*], Pedro Navarro-Santos[2*]

[1]Instituto de Investigaciones Químico-Biológicas, Universidad Michoacana de San Nicolás de Hidalgo, Morelia, México
[2]Investigadores por México, Universidad Michoacana de San Nicolás de Hidalgo, Morelia, México
Email: *rafael.herrera.bucio@umich.mx, *pnavarrosa@conahcyt.mx

How to cite this paper: Santana-García, R., Aviña-Verduzco, J., Herrera-Bucio, R. and Navarro-Santos, P. (2024) S_EAr Mechanism of the Products of 1,2-Dimethoxybenzene and a Captodative Olefin: A Theoretical Approach. *Computational Chemistry*, **12**, 57-74. https://doi.org/10.4236/cc.2024.123003

Received: July 7, 2024
Accepted: July 28, 2024
Published: July 31, 2024

Abstract

In this work, a conceptual DFT investigation is carried out to study the electrophilic aromatic substitution reaction (S_EAr) of 1,2-dimethoxybenzene and 3-(*p*-nitrobenzoyloxy)-but-3-en-2-one (a captodative olefin). Herein, we have studied the regioselectivity of such reactions considering the effect of solvents of different polarities and the presence of BF_3 as the catalyst. Understanding the effect of the solvent and the role of the Lewis catalyst on the pathway of Friedel-Crafts reactions is important to further facilitate the introduction of side chains in aromatic rings with captodative olefins, and thus be able to synthesize compounds analogous to natural products, e.g., *α*-asarone. Global and local reactivity descriptors were obtained, finding a key role when these reactions take place in the presence of nonpolar solvents. In addition, the Intrinsic Reaction Coordinate diagrams (IRCs) were calculated. Such results of the free activation energy ($\Delta G^{\ddagger}$) clearly show that this reaction is entirely regioselective, forming the unique product in the *para* position, in agreement with our predictions of the local reactivity descriptors obtained from the Parr functions, wherein the first reaction step, the carbon C_4 of the aromatic compound 1,2-dimethoxybenzene is favored. Moreover, from the IRCs, we found that the reactivity of the *para* adduct increases in the presence of nonpolar solvents. Interestingly, considering a polar solvent (MeCN), the intermediate formed (*σ*-complex) is more stable since it presents a more significant charge transfer with the solvent than the intermediate in the presence of a nonpolar solvent, making a reaction more challenging to reach when the reaction is carried out in the presence of MeCN because of the increasing of the energetic barrier from *σ*-complex to the TS_2 in the intrinsic reactive coordinate diagram. Therefore, the polarity of the solvent plays an important role, particularly in the

activation energy of the TS_2. Our computational results explained our experimental results quite well, confirming the importance of the solvent's polarity to this S_EAr reaction and explaining why, experimentally, the nonpolar solvent drove the reaction under catalyzed conditions.

Keywords

Captodative Olefins, IRC, Alkylation, HSAB, S_EAr

1. Introduction

The alkylation of aromatic compounds is a chemical reaction in which an alkyl group is added to an aromatic ring. This process can be carried out by electrophilic aromatic substitution reactions (S_EAr), very versatile reactions majorly employed for the formation of a C-C bonding promoted by a Lewis acid as the catalyst, where an alkyl group replaces a hydrogen atom of the aromatic ring through the interaction of an alkylating agent, e.g., an electron-deficient substituted alkene [1]-[3].

Within the electron-deficient alkenes, the captodative olefins (Cd-O) are highly reactive compounds because of the way the double bond is geminally substituted, *i.e.*, an attracting group and an electron-donor group that stabilizes the electronic charge of the system; both groups attached to the same double bond. The captodative effect makes Cd-O especially selective; in such a way, they are considered a model for studying electronic effects because they possess an attracting/donor group of electron density in their structure. These olefins have been used in organic synthesis as dienophiles in Diels-Alder cycloaddition reactions [4] [5] and Friedel-Crafts type Michael addition reactions with which naturally occurring compounds with therapeutic properties have been synthesized [6] [7].

The *α*-ketols nuclear structures of Cd-O, such as 3-(*p*-nitrobenzoyloxy)-but-3-en-2-one (**1**) combined with aromatic heterocyclic or functionalized aromatic rings, are employed for the organic synthesis of various naturally occurring and pharmacologically active compounds. Transformation of organic compounds has been mainly used in synthesizing products generally recognized as building blocks for preparing important natural and non-natural target molecules [7] [8].

Reliable information about the reactivity and selectivity of involved species in an efficiently electrocyclic reaction has been described, e.g., employing the frontier-molecular-orbital (FMO) [9], electron localization function (ELF) [10], Parr [11] and Fukui functions, and global descriptors based on the HSAB principle [12], so that, it is possible to understand the intrinsic mechanism of the formations of products involving Cd-O.

In a preview report, we reported the olefins synthesis: 1-acetyl vinyl *p*-arenecarboxylates [1] and alkyl 2-aroyloxy acrylates [9], where the Diels-Alder (DA) products and 1,3-dipolar cycloadditions have shown highly reactive and selective. Moreover, 1-acetyl vinyl *p-arene carboxylates* are highly reactive and selective in

Friedel-Crafts reactions [6]. The electrocyclic mechanism of the electrophilic aromatic substitution of activated benzenes with the captodative olefin 1-acetylvinyl-1-*p*-nitrobenzoate was successfully evaluated through the conceptual DFT descriptors, e.g., global reactivity descriptors, Parr functions, Fukui functions and the dual descriptors along the intrinsic reactive coordinates [1].

In addition, the hard and soft acids and bases (HSAB) principle was applied as a new approach to elucidate the reactive and selective of the 1-acetyl vinyl *p-arene carboxylates* [13]. In this context, we proposed an understanding of the reactivity by applying Hard-Soft Acid-Base and DFT calculations to rationalize the preferential selectivity of the electrophilic aromatic substitution.

In this work, we present a computational study based on descriptive DFT calculations of the intrinsic reaction coordinate of the electrophilic aromatic substitution of the aromatic compound (1,2-dimethoxybenzene, **2**) with the captodative olefin 3-(*p*-nitrobenzoyloxy)-but-3-en-2-one (**1**) in the presence of BF_3 as the catalyst including the effect of some solvent conditions *i.e.*, *n*-hexane and acetonitrile (MeCN) according to the reaction shown in Scheme 1 to obtain the products **3** and **4**, respectively. Experimental details and the NMR spectra are included in the Supporting Information. It is worth mentioning that the unique product obtained experimentally was **3** (80% yield) in the presence of *n*-hexane as the solvent. According to our findings obtained from this work, we can discern the role played by the solvent in the intrinsic reactivity of reagents, as well as the regioselectivity of the reaction.

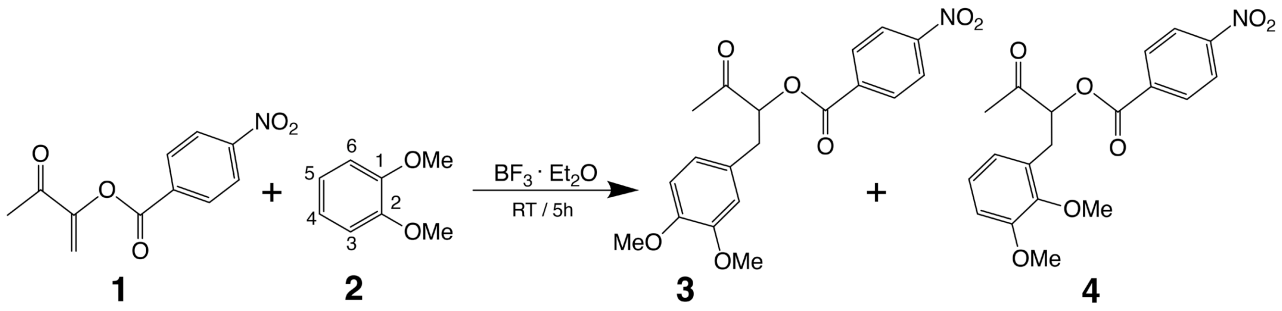

Scheme 1. The S_EAr reaction of the Cd-O (**1**) and 1,2-dimethoxybenzene (**2**).

2. Computational Details

The geometries of critical points, *i.e.*, reagents, intermediates of reactions, transition states (TSs), and products of the studied reactions, were found from Density Functional Theory calculations at the level of theory M062X/6-311++G (d, p) in Gaussian 16 [14]. Such a level of theory compromises a good approximation in terms of spent computational time and precision, which includes long-range and dispersion terms [15]. Other levels of theory were explored to calculate the energetic barriers, e.g., by using the triple zeta basis set of Barone [16], which includes diffuse functions, double *d*-polarizations, and a single set of *f*-polarization functions, we did not find significant differences that would change the role of the

solvents nor considerable decrease of the energetic barriers (see Table S1 of the supporting information for details). The TS geometries were found by applying Schelegel's synchronous transit-guided quasi-Newton method (QST3) and confirmed as first-order saddle points with only one negative eigenvalue (see Table S1 of the Supporting Information for details).

Meanwhile, reagents, intermediates, and products were verified with frequency calculations to be stable structures. To confirm that such TSs connect reagents and products, the IRC calculations were carried out at the described level of theory (see Figure S4 and Figure S5 for details). Solvent effects were considered for the implicit solvation model using the Polarizable Continuum Model (PCM) using *n*-hexane and acetonitrile (MeCN).

The electronic structures of the transition states and intermediates were analyzed quite well through electrophilic and nucleophilic indices by calculating the dual descriptor [17] and the electron localization function (ELF), respectively.

Global reactivity descriptors are analyzed to understand the nature of the S_EAr reaction, as defined in the conceptual DFT. The chemical potential (μ) is calculated by using the following equation 1, where I and A are the ionization potential and the electron affinity of a chemical species, respectively:

$$\mu \approx -\frac{I+A}{2} \tag{1}$$

For our calculations, both I and A values were approximated as the negative of the highest occupied molecular orbital energy (HOMO) and the lowest unoccupied molecular orbital energy (LUMO), respectively. Hardness (η) is computed as the difference between the values of I and A; meanwhile, the global softness (S) is approximately the inverse of η. The global electrophilicity index is computed according to its definition [18]:

$$\omega = \frac{\mu^2}{2\eta} \tag{2}$$

The nucleophilicity index (N) is defined as the difference between a chemical species and the HOMO energy of tetracyanoethylene as a reference [10] to maintain N on a positive scale. The values of the free Gibbs energy of each species were obtained at 298 K and 1 atm from the harmonic vibrational frequencies calculated at the same level of theory described above through the following equation:

$$G_{corr} = E_{tot} + k_B T - TS_{tot} \tag{3}$$

Here, E_{tot} is the thermal correction to energy, k_B is the Boltzmann constant, and S_{tot} is the total entropy contribution. To calculate the energetic barriers reaching the TS_1, the sum of the free Gibbs energy of separate reagents is taken as a reference.

3. Results and Discussion

3.1. Global Reactivity Indices of Reagents

The global reactivity indices μ, η, S, ω, and N of reagents **1 and 2** and their

coordinated forms with BF_3 are presented in Table 1. By examining the μ values, we noticed that the presence of the catalyst decreases the chemical potential of the Cd-O and the aromatic compound concerning their non-coordinated forms. Values of hardness increase in the coordinated species of both reagents and decrease concerning the polarity of solvents. It is worth mentioning that the electrophilicity of reagents increases because of the catalyst's presence and the polarity of solvents.

Table 1. Global reactivity descriptors [in eV] of **1**, **2** and their BF_3-coordinated forms in the gas phase, *n*-hexane, and MeCN, respectively.

Gas phase					
	μ	η	S	ω	N
1	−5.80	8.48	0.06	1.99	1.47
1-BF$_3$	−6.42	8.83	0.06	2.33	0.84
2	−3.82	9.06	0.06	0.80	3.42
2-BF$_3$	−4.30	9.55	0.05	0.97	2.67
***n*-hexane**					
	μ	η	S	ω	N
1	−5.72	6.66	0.08	2.46	1.34
1-BF$_3$	−6.17	7.10	0.07	2.69	0.94
2	−3.65	7.61	0.07	0.88	3.22
2-BF$_3$	−4.09	8.02	0.06	1.04	2.57
MeCN					
	μ	η	S	ω	N
1	−5.66	4.67	0.11	3.43	1.11
1-BF$_3$	−5.87	4.85	0.10	3.55	1.07
2	−3.61	5.91	0.08	1.10	2.84
2-BF$_3$	−4.07	5.95	0.08	1.39	2.37

From Table 1, we also noticed that the most nucleophilic species found for these reactions is the non-coordinated aromatic compound in the presence of a nonpolar solvent, *i.e.*, in this case, *n*-hexane. The global reactivity descriptors results suggested that the most electrophilic form of the Cd-O may be its coordinated form in the presence of polar solvents. However, **1-BF$_3$** in a non-polar solvent is the most favored species regarding the electrophilicity generated when coordinating with BF_3 compared to any other solvent polarity. Meanwhile, the non-coordinated aromatic compound (2) in a nonpolar solvent is the better nucleophile. Moreover, chemical hardness (η) increases because of the presence of the catalyst for both reagents. However, η decreases as the polarity of the solvents for both the electrophilic and the nucleophilic reagents. Indeed, we observed that the pair **2/1-BF$_3$** in the presence of *n*-hexane might be more favorable to react concerning the other solvents since the hardness values are very close, following the HSAB principle [12].

We calculated the difference in the chemical potential ($\Delta\mu$) shown in Table 2 to determine how these reactions may occur. Although the MeCN solvent is important to increase the electrophile character of the Cd-O, the most significant $\Delta\mu$ value is found for the pair **2/1-BF$_3$** in the presence of *n*-hexane as the solvent, in agreement with our calculated values of η for the pair **2/1-BF$_3$** in the presence of *n*-hexane, whose reactivity increases according to the HSAB principle. Moreover, the most nucleophilic form of **2** is predicted under nonpolar. We also noticed that the $\Delta\mu$ values decreased concerning the polarity of the studied solvents. Our findings indicate that the global electron density transfer (GEDT) [19] along these reactions will occur from the 1,2-dimethoxybenzene and the coordinated form of the Cd-O. In addition, we calculated the energetic free energy barriers employing QST3 calculations to coordinate BF_3 and **1**, finding that the coordination in the presence of MeCN has a higher energetic cost than that of *n*-hexane (see Table S3 in the Supporting Information for details).

Table 2. The difference in the chemical potential ($\Delta\mu$) for the reaction between **2/1**, **2/1-BF$_3$**, **2-BF$_3$/1**, and **2-BF$_3$/1-BF$_3$** [in eV] in the gas phase, *n*-hexane, THF, and MeCN, respectively.

	Gas	*n*-hexane	THF	MeCN
2/1	1.99	2.07	2.10	2.04
2/1-BF_3	2.61	2.52	2.36	2.25
2-BF_3/1	1.51	1.63	1.60	1.59
2-BF_3/1-BF_3	2.13	2.08	1.87	1.80

These findings explain why we obtained only a reaction product in the presence of nonpolar solvents. Regardless of the product to be formed, the regioselectivity of the reaction will be addressed in the following paragraphs. Moreover, it will show evidence to explain why only product **3** is observed experimentally.

3.2. Local Reactivity Descriptors

To give insight into the relative activation of carbons of **2**, the local reactivity of the regioselective carbons of **2** was analyzed by using the nucleophilicity Parr functions [11] (P_k^+) and the local nucleophilicity index (N_k) based on the spin density distribution at the radicals and a neutral molecule, which have been described the regio- and chemoselectivity in this kind of reactions successfully [11]. Moreover, those descriptors have been developed, explaining a charge transfer process quite well.

For this reaction, Table 3 shows the values of P_k^+ and N_k of the regioselective center of **2**. One might expect this reaction would have a higher yield of **3** more than **4** because of the competitivity on the C_3 or C_4, respectively. However, our results demonstrated a high selectivity toward C_4 of **2** finding the most significant difference between the P_{c3}^+ and P_{c4}^+ sites when the nonpolar solvent is considered.

Table 3. Local Nucleophilicity indices of **2**: Nucleophilic Par function (P_k^+) and local nucleophilicity (N_k), respectively, calculated in the gas phase, n-hexane, THF, and MeCN as a solvent.

		Gas phase		*n*-hexane		THF		MeCN	
		P_k^+	N_k	P_k^+	N_k	P_k^+	N_k	P_k^+	N_k
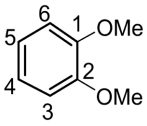	$k = C_3$	0.024	0.081	0.032	0.101	0.042	0.123	0.045	0.129
	$k = C_4$	0.199	0.681	0.212	0.681	0.227	0.668	0.233	0.661
	ratio (C_3/C_4)			6.62	6.74	5.40	5.43	5.17	5.12

On the other hand, the local nucleophilicity on C_3 slightly increases with respect to the polarity of the solvent. However, the local nucleophilicity of C_4 is much larger than C_3. Indeed, the most significant ratio between values of the nucleophilicity indices of C_4 is up to 6.74 times larger than C_3, found when *n*-hexane is considered. These results may explain our experimental observations that only product **3** is characterized by nonpolar solvents.

3.3. Intrinsic Reaction Coordinates

Once the reactivity of **1** and **2** was analyzed according to their global and local reactivity descriptors for these S_EAr, the Intrinsic Reaction Coordinate (IRCs) calculations were carried out, where only the critical points are presented (*i.e.*, reaction intermediaries and TSs) for the reaction of **2** and **1-BF$_3$** to form **3** and **4**, respectively. Figure 1(a) shows the two-step reaction mechanism and the Gibbs free activation energy ($\Delta G^{\ddagger}$) along the formation of **3**, representing the most probable reaction that may occur. The energetic barriers of the pathway for forming **4** are also included in Figure 1(b) for comparison. Such IRCs were calculated in nonpolar and polar solvents, respectively. Details of the critical points of the studied IRCs are included in the Supporting Information as a reference.

Figure 1(a) shows that the reaction to form **3** is energetically favored in the presence of *n*-hexane more than MeCN because the energetic barriers of both TSs when the non-polar solvent is used are lower than those considering MeCN. The calculated values for such stationary points are $\Delta G_{Ts1} = 12.9$ and $\Delta G_{Ts2} = 14.6$ kcal·mol^{-1} in the presence of *n*-hexane and $\Delta G_{Ts1} = 16.7$ and $\Delta G_{Ts2} = 20.2$ kcal·mol^{-1} considering MeCN, respectively. Moreover, our calculations suggested that the limiting step in such IRC is the TS_2, given that they present the maximum free independent of the nature of the solvents. However, in *n*-hexane, the energy barrier of TS_2 is 5.7 kcal·mol^{-1}, lower than when MeCN is considered the solvent.

In addition, the rate constant was calculated from the difference in the standard state-free energy between the limiting steps. Mainly, we focus on the energy barrier of TS_2 shown in Figure 1(a) (considering that **3** was the unique product observed experimentally) because this TS is located at the highest point of the reaction coordinate diagram. Therefore, it can be considered the determining step of the kinetics of the reaction. We calculated the $k_{forward}$ and $k_{reverse}$ [20] to

determine the displacement to products and reactants, respectively, and then the rate constant was determined. In the presence of *n*-hexane $K_{eq} = 4.5\times10^{-22}$ while in acetonitrile $K_{eq} = 2.3\times10^{-30}$. These results do not present any discrepancy with the experimental observations, *i.e.*, **3** was obtained as the unique product only in the presence of *n*-hexane as a solvent, which is also kinetically favored.

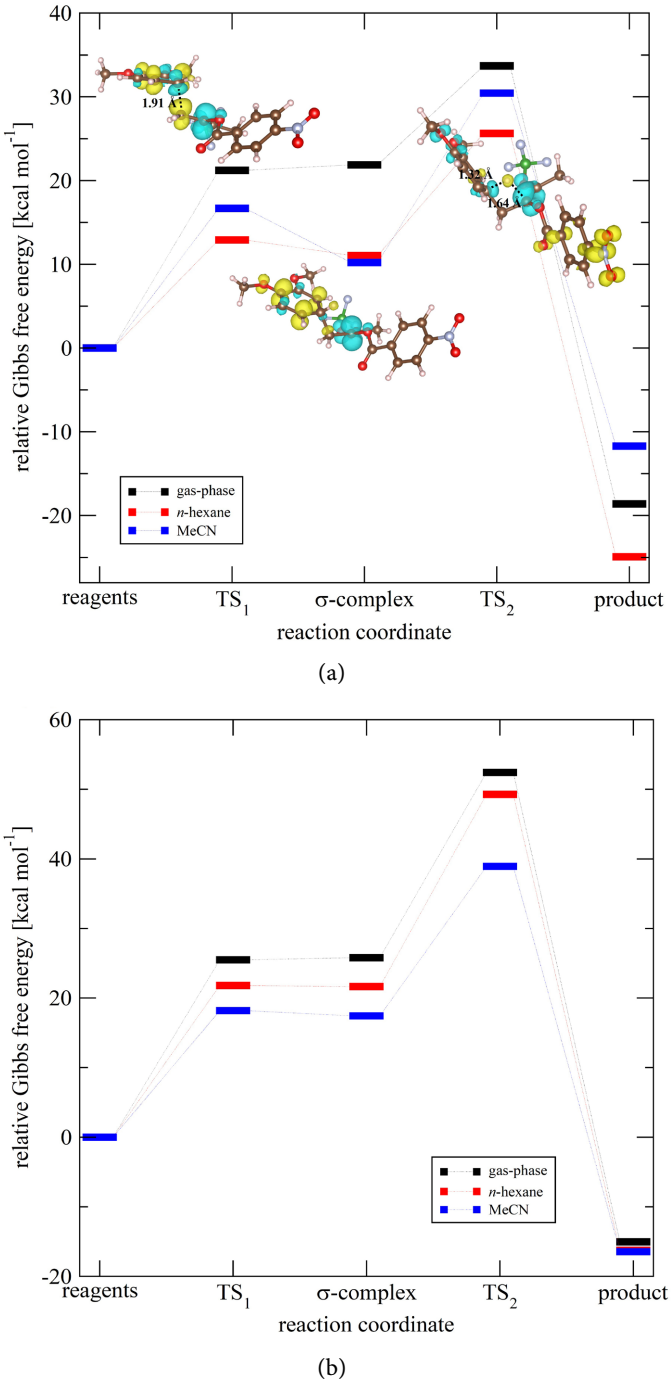

Figure 1. The IRCs for forming adducts (a) **3** and (b) **4**. They were calculated at the gas phase (black bars) in the presence of *n*-hexane (red bars) and MeCN (blue bars) as the solvents, respectively.

To investigate the influence of the polarity of the solvent during the reaction mechanism, we calculated the partial charge of the carbons geminal (C_g) and terminal (C_T) of the Cd-O as well as charge of the carbon of the aromatic compound (C_4 considering the formation of product **3**) forming the intermediate σ-complex (see Table S2). Such C atoms are directly involved during both studied IRCs. We compared their charges in the presence of solvents concerning the charges of such atoms in the gas phase. From these results, we found that the most significant charge transfer occurs in the presence of MeCN stabilizing the σ-complex; as a consequence, interestingly, the σ-complex is stabilized so that, as we can see, the TS_2 energy barrier is increased to 20.2 kcal·mol^{-1} for its intermediate.

For comparison, in Figure 1(b), we observed in the IRC to form **4** that the energetic barriers are higher in the TS_1 and TS_2 than in the IRC of **3** shown in Figure 1(a). Moreover, once TS_1 is reached, the energy difference for the formation of the σ-complex is minimal (~1 kcal·mol^{-1}), which could lead to important energy impediments following the reaction coordinate so that the formation of the σ-complex would be entirely reversible to reagents. Particularly, the energy barriers from the σ-complex to the TS_2 are ΔG_{TS2} = 27.6 kcal·mol^{-1} and 21.5 kcal·mol^{-1}, considering *n*-hexane and MeCN as the solvent, respectively. For this reason, we notice the difficulty of experimentally observing product **4**, even when the experiments were carried out in the presence of solvents of different polarities. On the other hand, the polarity of other solvents that could slightly stabilize the σ-complex could be further studied for the formation of **4** since it is observed in both IRCs of Figure 1 that TS_2 is the determinant stage of the reaction.

The reactivity of the critical points along the reaction coordinate of these reactions is presented by plotting the dual descriptor [17] to visualize in the same figure and molecule the areas rich in electron density (in blue) susceptible to an electrophilic attack and areas deficient in electron density (in yellow) susceptible to a nucleophilic attack.

In Figure 1(a), we can observe the global reaction coordinate diagram showing the pathway of the mechanism and the energetic cost of the two transition states. The first step corresponds to the formation of C_4 - C_T, where C_4 is the most nucleophilic carbon of **2** and C_T is the terminal carbon of the highest electrophilic behavior of **1-BF$_3$**. For the formation of the bonding C_4 - C_T, the electrons of C_4 are displaced towards carbon C_T following the TS_1, subsequently obtaining the zwitterionic intermediate (σ-complex). In the second stage, a proton migration occurs (hydrogen bonded to C_4) towards the geminal carbon (C_G) adjacent to C_T following the TS_2.

Figure 1(a) includes the isovalues of the dual descriptor, which help us visually demonstrate the reactivity of each step, e.g., in TS_1 of Figure 1(a), we can see that C_4 of **2** has a blue zone, indicating that it is susceptible to electrophilic attacks. On the other hand, we observe that C_T of **1-BF$_3$** has a yellow region. This suggests that it is susceptible to nucleophilic attacks. The areas mentioned above are to be expected since C_4 is effectively moving its electrons to the deficient region, which in this case is C_T.

During the formation of the σ-complex, we can observe that once C_4 moves its electrons to C_T, only a blue region is observed near C_G, which is expected because the electron density belonging to C_T is displaced to C_G, which is susceptible to electrophilic attacks.

In TS_2, we can observe a yellow region near the proton (bonded previously to C_4) and the blue zone of C_G. This helps us corroborate that it is indeed a transition state since C_G presents the electrons of C_T to form a bond with the proton.

3.4. Electron Localization Functions

The electron localization functions (ELF) analysis of the reaction between **2** and **1-BF$_3$** is presented in Figure 2 in the stationary points of the TS_1 and TS_2 to form **3**, plotted using the visualization program Chimera. From the populations of ELF basins, we can observe in the TS_1 a blue region indicating the dissipation of the electronic density; this is distributed (reshuffling of the charge distribution) from the MeO *ortho* to the aryl to the acyl of the captodative olefin passing through the geminal carbon. On the other hand, in the TS_2, the blue zone indicates the dissipation of the electronic density; this is distributed (electron reshuffling) from the MeO in the *ortho* position to the aryl to the acyl of the captodative olefin passing through the geminal carbon.

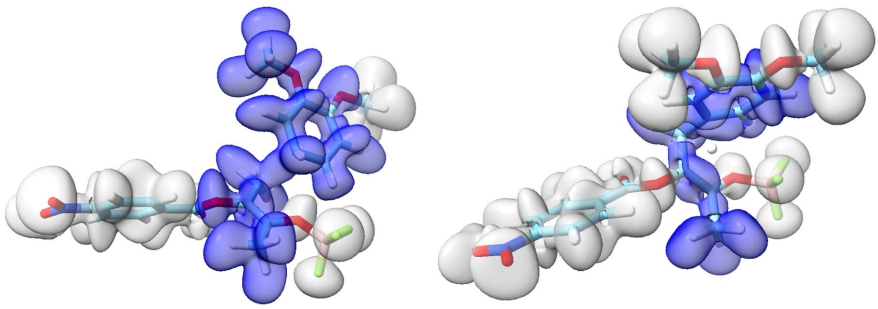

(a) (b)

Figure 2. ELF at the (a) TS_1 and (b) TS_2 stationary states for forming **3** in the presence of *n*-hexane as the solvent.

We assume that only these atoms participate in the charge transfer and the reshuffling of the charge distribution involved in the bond formation processes.

4. Conclusions

The regioselectivity of the reaction of the Cd-O in the presence of BF_3 as the catalyst and the 1,2-dimethoxybenzene has been studied in the framework of the DFT. The importance of nonpolar solvent for forming product **3** was demonstrated, finding that the limiting step of this reaction is the formation of the TS_2 independently of the studied solvent. One reason is the stabilization of the σ-complex because of the nature of the solvent, e.g., considering MeCN increases the energetic barrier to TS_2.

Analyzing the transition states for the most favored reaction through the isovalues of the dual descriptor and ELF results observed that the electron-deficient yellow region is susceptible to nucleophilic attacks, and the electron-rich blue areas which are liable to electrophilic attacks, and the participation of the MeO *ortho* to the aryl to the acyl of the captodative olefin passing through the geminal carbon in the dissipation of the electron density of the stationary states. These results provide important information about the reactivity of these S_EAr, the controlling steps, and the factors that drive their mechanism. Our results confirm the importance of the solvent's polarity to this S_EAr reaction, explaining why the nonpolar solvent drove the reaction under catalyzed conditions.

Conflicts of Interest

The authors declare no conflicts of interest regarding the publication of this paper.

References

[1] Morales-Palacios, F.G., Navarro-Santos, P., Beiza-Granados, L., Rivera, J.L., García-Gutiérrez, H.A. and Herrera-Bucio, R. (2019) Conjugate Addition between Syringol and a Captodative Olefin Catalyzed by BF3. *Journal of Physical Organic Chemistry*, **32**, e4011. https://doi.org/10.1002/poc.4011

[2] Evano, G. and Theunissen, C. (2019) Beyond Friedel and Crafts: Innate Alkylation of C-H Bonds in Arenes. *Angewandte Chemie International Edition*, **58**, 7558-7598. https://doi.org/10.1002/anie.201806631

[3] Crampton, M.R. (2014) Electrophilic Aromatic Substitution. In: Knipe, A.C., Ed., *Organic Reaction Mechanisms* 2011, Wiley, 257-283.

[4] Mertes, J. and Mattay, J. (1988) Captodative Olefins in Normal and Inverse *Diels-Alder* Reactions. *Helvetica Chimica Acta*, **71**, 742-748. https://doi.org/10.1002/hlca.19880710408

[5] Reyes, A., Aguilar, R., Munoz, A.H., Zwick, J.C., Rubio, M., Escobar, J.L., *et al.* (1990) Highly Selective Diels-Alder Cycloadditions of Captodative Dienophiles 1-Acetylvinyl Arenecarboxylates to Unsymmetrically Substituted Butadienes. *The Journal of Organic Chemistry*, **55**, 1024-1034. https://doi.org/10.1021/jo00290a039

[6] Aguilar, R., Benavides, A. and Tamariz, J. (2004) Friedel-Crafts Reaction of Activated Benzene Rings with Captodative and Electron-Deficient Alkenes. A One-Step Synthesis of the Natural Product Methyl 3-(2,4,5-Trimethoxyphenyl)propionate. *Synthetic Communications*, **34**, 2719-2735. https://doi.org/10.1081/scc-200026193

[7] Zárate-Zárate, D., Aguilar, R., Hernández-Benitez, R.I., Labarrios, E.M., Delgado, F. and Tamariz, J. (2015) Synthesis of A-Ketols by Functionalization of Captodative Alkenes and Divergent Preparation of Heterocycles and Natural Products. *Tetrahedron*, **71**, 6961-6978. https://doi.org/10.1016/j.tet.2015.07.010

[8] Cardillo, G. and Tomasini, C. (1996) Asymmetric Synthesis of β-Amino Acids and α-Substituted β-Amino Acids. *Chemical Society Reviews*, **25**, 117-128. https://doi.org/10.1039/cs9962500117

[9] Herrera, R., Jiménez-Vázquez, H.A., Modelli, A., Jones, D., Söderberg, B.C. and Tamariz, J. (2001) Synthesis of New Captodative Alkenes: Alkyl 2-Aroyloxy Acrylates—Structure, and Reactivity in Diels–Alder Cycloadditions. *European Journal of Organic Chemistry*, **2001**, 4657-4669. https://doi.org/10.1002/1099-0690(200112)2001:24<4657::aid-ejoc4657>3.0.co;2-3

[10] Domingo, L.R., Chamorro, E. and Pérez, P. (2008) Understanding the Reactivity of Captodative Ethylenes in Polar Cycloaddition Reactions. A Theoretical Study. *The Journal of Organic Chemistry*, **73**, 4615-4624. https://doi.org/10.1021/jo800572a

[11] Domingo, L.R., Pérez, P. and Sáez, J.A. (2013) Understanding the Local Reactivity in Polar Organic Reactions through Electrophilic and Nucleophilic Parr Functions. *RSC Advances*, **3**, 1486-1494. https://doi.org/10.1039/c2ra22886f

[12] Pearson, R.G. (1963) Hard and Soft Acids and Bases. *Journal of the American Chemical Society*, **85**, 3533-3539. https://doi.org/10.1021/ja00905a001

[13] Poon, T., Mundy, B.P. and Shattuck, T.W. (2002) The Michael Reaction. *Journal of Chemical Education*, **79**, 264. https://doi.org/10.1021/ed079p264

[14] Frisch, M.J., Trucks, G.W., Schlegel, H.B., Scuseria, G.E., Robb, M.A., Cheeseman, J.R., *et al.* (2016) Gaussian 16 Rev. C.01. Wallingford, CT.

[15] Zhao, Y. and Truhlar, D.G. (2007) The M06 Suite of Density Functionals for Main Group Thermochemistry, Thermochemical Kinetics, Noncovalent Interactions, Excited States, and Transition Elements: Two New Functionals and Systematic Testing of Four M06-Class Functionals and 12 Other Functionals. *Theoretical Chemistry Accounts*, **120**, 215-241. https://doi.org/10.1007/s00214-007-0310-x

[16] Barone, V. (1995) Structure, Magnetic Properties and Reactivities of Open-Shell Species from Density Functional and Self-Consistent Hybrid Methods. In: Chong, D.P., Ed., *Recent Advances in Computational Chemistry*, World Scientific Publishing, 287-334. https://doi.org/10.1142/9789812830586_0008

[17] Morell, C., Grand, A. and Toro-Labbé, A. (2004) New Dual Descriptor for Chemical Reactivity. *The Journal of Physical Chemistry A*, **109**, 205-212. https://doi.org/10.1021/jp046577a

[18] Parr, R.G., Szentpály, L.v. and Liu, S. (1999) Electrophilicity Index. *Journal of the American Chemical Society*, **121**, 1922-1924. https://doi.org/10.1021/ja983494x

[19] Domingo, L.R. (2014) A New C-C Bond Formation Model Based on the Quantum Chemical Topology of Electron Density. *RSC Advances*, **4**, 32415-32428. https://doi.org/10.1039/c4ra04280h

[20] Tavakol, H. and Arshadi, S. (2009) Theoretical Investigation of Tautomerism in N-Hydroxy Amidines. *Journal of Molecular Modeling*, **15**, 807-816. https://doi.org/10.1007/s00894-008-0435-4

Supporting Information

To carry out the reaction described in Scheme 1, 0.50 g (0.0021 moles) of **1** and 0.88 g (0.0063 moles) of **2** were mixed using *n*-hexane (5 ml) as a solvent, and $BF_3{\cdot}Et_2O$ (0.15 ml) as the catalyst under magnetic stirring for 5 h of reaction at room temperature. Obtaining **3** as the unique product (80% yielding). From the residue, **3** was purified using a chromatographic column using a hexane-ethyl acetate mixture (4:1).

Through the ^{1}H-NMR spectrum at 400 MHz using $CDCl_3$ as a solvent (Figure S1) was acquired the chemical shifts (δ) of 2.17 (s, 3H, H-1), 3.15 (dd, J = 14.4, 8.0 Hz, 1H, H-4_{trans}), 3.23 (dd, J = 14.4, 5.1 Hz, 1H, H-4_{cis}), 3.85 (s, 3H, H-16), 3.86 (s, 3H, H-16), 5.46 (dd, J = 8.0, 5.1 Hz, 1H, H-3), 6.77 (s, 1H, H-10), 6.81 (d, 2H, H-6 y H-7), 8.20 (d, J = 9.0 Hz, 2H, H-13, 13'), 8.30 (d, J = 9.0 Hz, 2H, H-14, 14'). Where H-10 was observed as a single signal, H-6 and H-7 were double signals, confirming that the structure of **3** is the unique product. It was necessary to analyze the two-dimensional HETCOR spectrum (Figure S2) to support the assignment of hydrogens.

According to the literature, the C spectrum of product **3** at 100 MHz using $CDCl_3$ as a solvent (Figure S3), shows the chemical shifts (δ) of 27.3 (C-1), 36.5 (C-4), 80.8 (C-3), 111.2 (C-6), 112.5 (C-10), 121.4 (C-7) 123.7 (C-14), 128.0 (C-5), 130.9 (C-13), 148.8 (C-12), 151.1 (C-15), 163.9 (C-11), 204.6 (C-2) (Tables S1-S3, Figure S4, Figure S5).

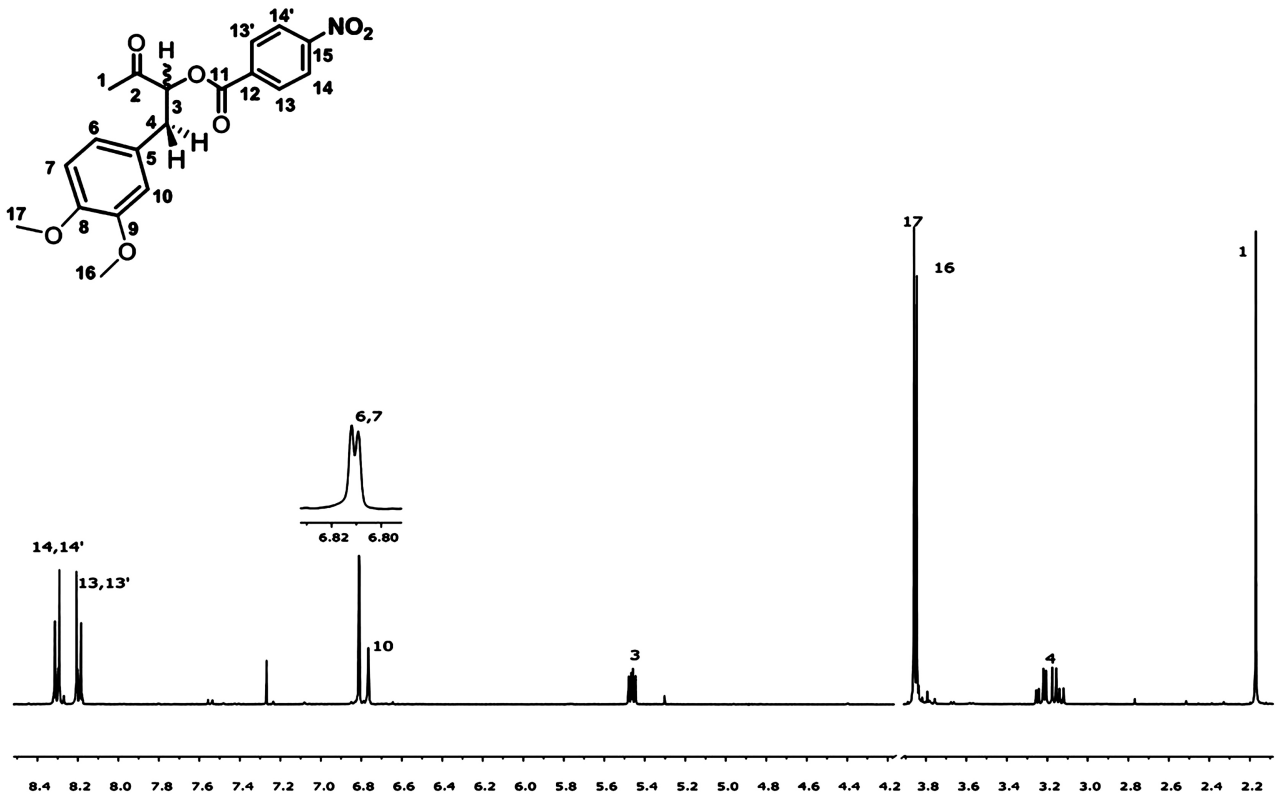

Figure S1. ^{1}H-NMR spectrum at 400 MHz of **3**.

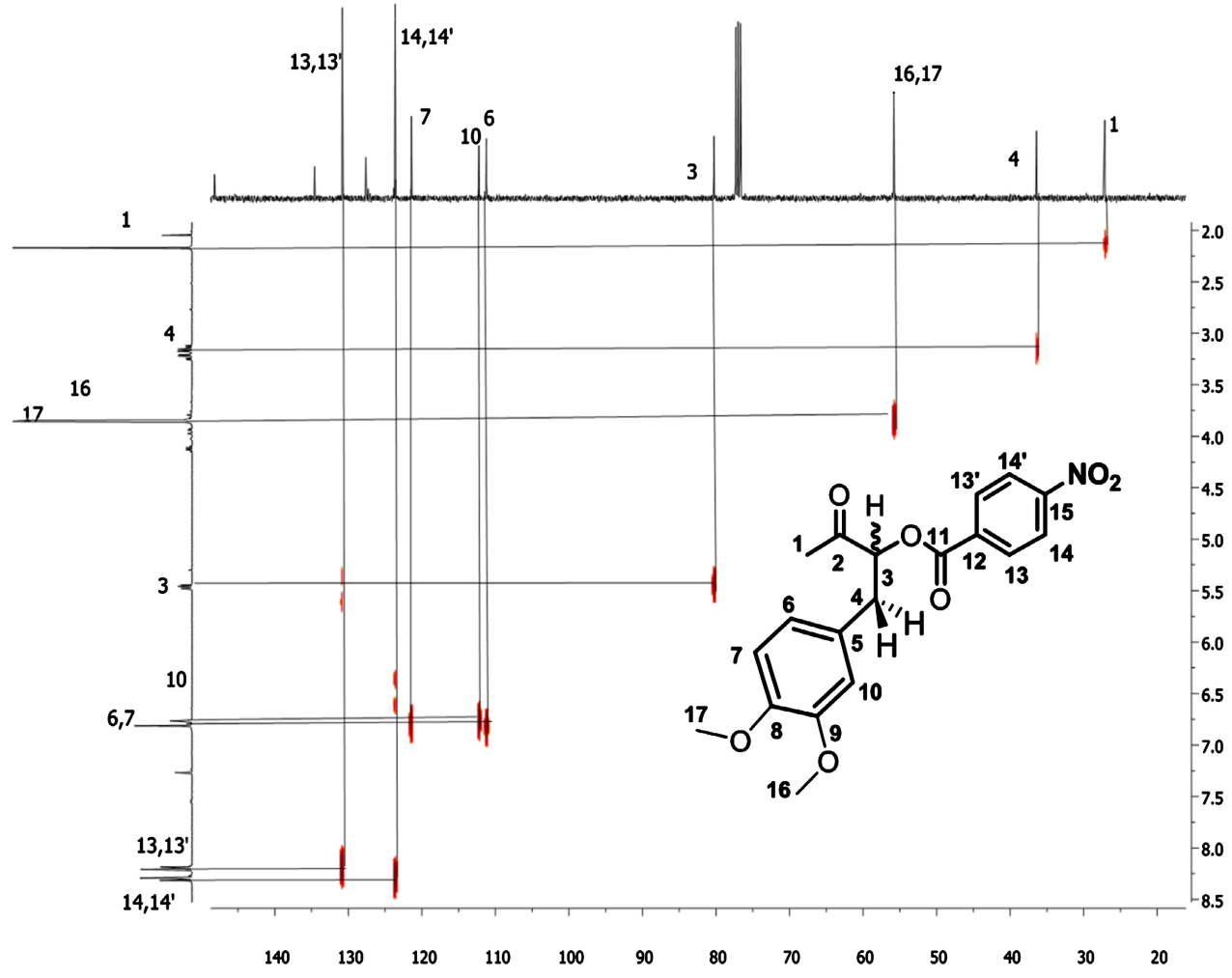

Figure S2. HETCOR spectrum of **3**.

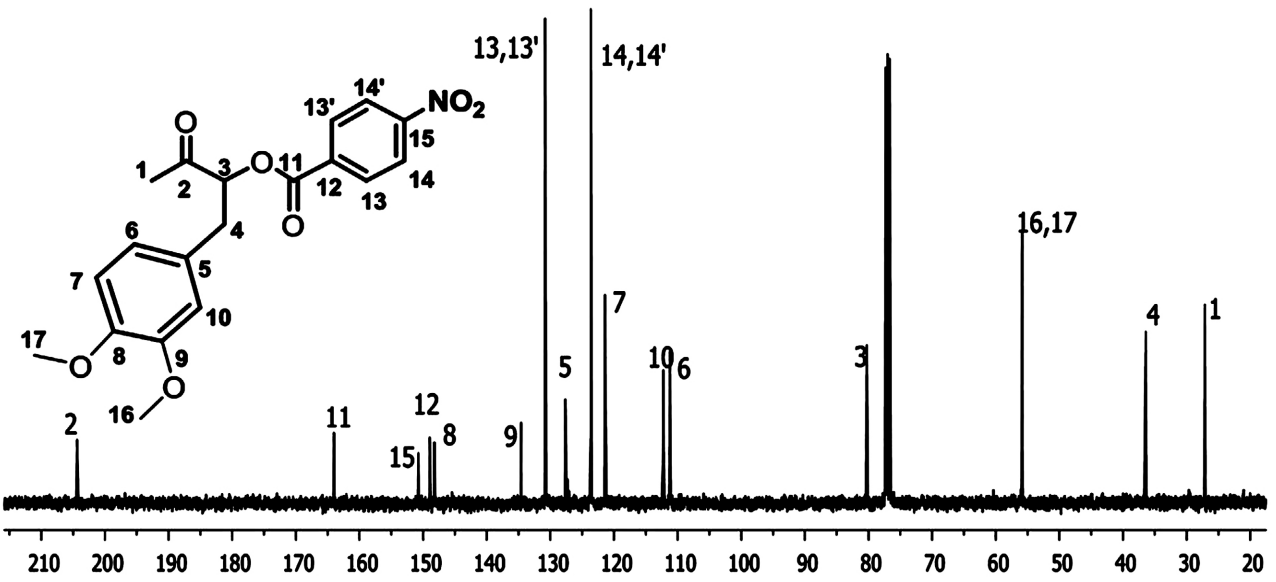

Figure S3. ^{13}C NMR spectrum of **3**.

Table S1. Gibbs free energy (ΔG, in kcal·mol^{-1}) of the stationary points involved in the reaction between **2** and **1-BF$_3$** to form the adducts *para* (**3**) and *meta* (**4**) respectively. Calculations were done employing two different level of theory, computed in the gas-phase, *n*-hexane, and MeCN, imaginary frequencies are shown in brackets for the characterized transition states.

		(ΔG)					
		M062X/PCM/6-311++g (d, p)			M062X/PCM/EPR-III		
		Gas-phase	*n*-hexane	MeCN	Gas-phase	*n*-hexane	MeCN
yielding the product **3**	TS_1	21.2 (−383.6)	12.9 (−405.9)	16.7 (−400.8)	24.5 (−312.29)	16.1 (−399.41)	17.2 (−430.17)
	σ-complex	21.9	11.1	10.2	25.0	14.5	11.0
	TS_2	33.7 (−850.4)	25.6 (−966.8)	30.4 (−1106.9)	36.3 (−1047.76)	28.6 (−1172.53)	31.0 (−1348.39)
	Products	−18.6	−24.9	−15.0	−16.6	−22.3	−17.1
yielding the product **4**	reagents						
	TS_1	25.5 (−383.7)	21.8 (−407.5)	18.2 (−433.2)	25.4 (−325.66)	23.6 (−363.23)	18.7 (−409.15)
	σ-complex	25.8	21.6	17.4	25.9	23.3	17.9
	TS_2	52.4 (−1042.5)	49.5 (−1163.6)	38.9 (−1351.2)	52.1 (−1295.00)	50.5 (−1386.87)	33.0 (−1370.42)
	Products	−16.2	−16.2	−16.5	−14.3	−14.0	−15.1

Table S2. Atomic charges of involved C atoms to form the *σ-complex* in the IRC of product **3** considering *n*-hexane and MeCN as the solvent.

	i	gas-phase	*n*-hexane	MeCN	Δq^i_{hex}	Δq^i_{MeCN}
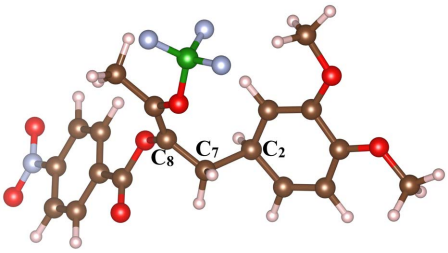	C_2	−0.62	−0.59	−0.50	0.03	0.12
	C_7	0.74	0.62	0.48	−0.12	−0.27
	C_8	−0.11	0.04	0.22	0.15	0.34

Table S3. Gibbs free energy (ΔG, in kcal·mol^{-1}) of the stationary points involved in coordinating **1** and BF_3 (BF_3OEt_2) to obtain the coordinated complex **1-BF$_3$**. Calculations were done employing two different levels of theory, computed in the gas-phase, *n*-hexane, and MeCN, imaginary frequencies are shown in brackets for the characterized coordination processes (transition state).

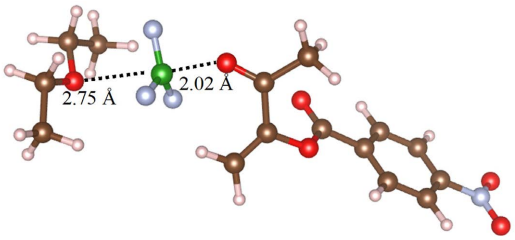	(Δ*G*)					
	M062X/PCM/6-311++g (d, p)			M062X/PCM/EPR-III		
	Gas-phase	*n*-hexane	MeCN	Gas-phase	*n*-hexane	MeCN
Reagents (BF_3-OEt_2 + **1**)	-	-	-	-	-	-
TS (coordination process)	4.3 (−149.73)	6.2 (−173.96)	7.9 (−176.26)	4.5 (145.3)	4.7 (−167.49)	19.0 (−102.98)
Products **1-BF$_3$** + OEt_2	−2.6	−2.6	−3.0	−6.2	−8.0	−9.8

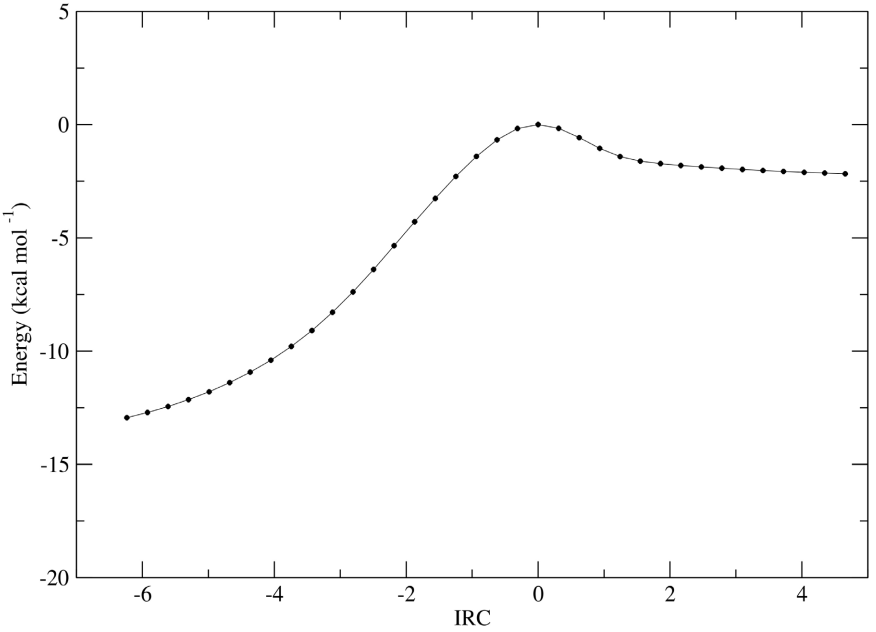

Figure S4. IRC pathway for TS_1 of the reaction to obtain **3**, considering *n*-hexane as the solvent. Potential energies (kcal·mol^{-1}) relative to the maximum (TS_1 energy).

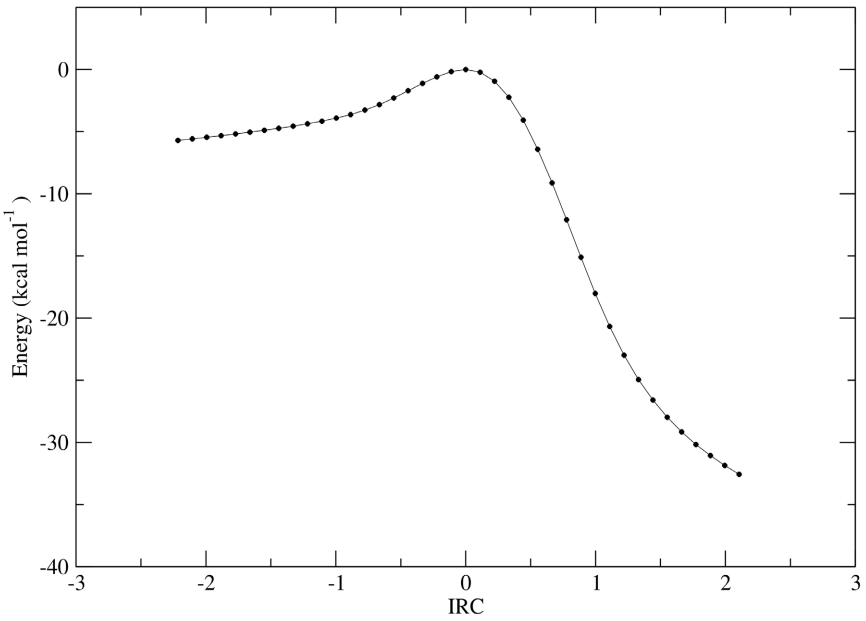

Figure S5. IRC pathway for TS_2 of the reaction to obtain **3**, using *n*-hexane as the solvent. Potential energies (kcal·mol^{-1}) relative to the maximum (TS_2 energy).

Coordinates along the IRC to connect reactants (**2** and **1-BF$_3$**) and product minima (*σ-complex*, in this case) *via* TS_1.

***n*-hexane:**

Total Energy along IRC

X-Axis: Intrinsic Reaction Coordinate

Y-Axis: Total Energy (Hartree)

#	X	Y
	−6.2354600000	−1641.0695399200
	−5.9237800000	−1641.0691755100
	−5.6120700000	−1641.0687564200
	−5.3003400000	−1641.0682740300
	−4.9886100000	−1641.0677184100
	−4.6768600000	−1641.0670783600
	−4.3651200000	−1641.0663419700
	−4.0533900000	−1641.0654956900
	−3.7416700000	−1641.0645259200
	−3.4299500000	−1641.0634113400
	−3.1182100000	−1641.0621323500
	−2.8064500000	−1641.0606899800
	−2.4946700000	−1641.0591105300
	−2.1828600000	−1641.0574430100
	−1.8710200000	−1641.0557579300
	−1.5591700000	−1641.0541168100
	−1.2473400000	−1641.0525641700
	−0.9355200000	−1641.0511582800
	−0.6237100000	−1641.0499914000
	−0.3119100000	−1641.0491991100
	0.0000000000	−1641.0489203800
	0.3118600000	−1641.0491814300
	0.6235800000	−1641.0498339000
	0.9349400000	−1641.0505924500
	1.2439100000	−1641.0511678600
	1.5490200000	−1641.0514876400
	1.8558600000	−1641.0516682700
	2.1641400000	−1641.0517917500
	2.4750400000	−1641.0518945000
	2.7867300000	−1641.0519869100
	3.0985500000	−1641.0520707600
	3.4103700000	−1641.0521465800
	3.7221800000	−1641.0522149100
	4.0339600000	−1641.0522763600
	4.3456900000	−1641.0523316900
	4.6573700000	−1641.0523817900
	4.9690100000	−1641.0524276500

Coordinates along the IRC to connect reactant (*σ-complex*, in this case) and product minima (**3**) *via* TS_2.

***n*-hexane:**

Total Energy along IRC

X-Axis: Intrinsic Reaction Coordinate

Y-Axis: Total Energy (Hartree)

#	X	Y
	−2.2155300000	−1641.0345288800
	−2.1046400000	−1641.0343334900
	−1.9937600000	−1641.0341315900
	−1.8828800000	−1641.0339222500
	−1.7720100000	−1641.0337042000
	−1.6611500000	−1641.0334758300
	−1.5503000000	−1641.0332349600
	−1.4394800000	−1641.0329786600
	−1.3286700000	−1641.0327028500
	−1.2179200000	−1641.0324016000
	−1.1072400000	−1641.0320655200
	−0.9966700000	−1641.0316786000
	−0.8861800000	−1641.0312147300
	−0.7756400000	−1641.0306407500
	−0.6649700000	−1641.0299333000
	−0.5542000000	−1641.0290975800
	−0.4433800000	−1641.0281703200
	−0.3325400000	−1641.0272123700
	−0.2217000000	−1641.0263966400
	−0.1108400000	−1641.0257131100
	0.0000000000	−1641.0254382700
	0.1109000000	−1641.0257895800
	0.2217800000	−1641.0269495100
	0.3326800000	−1641.0290037600
	0.4435800000	−1641.0319407300
	0.5544700000	−1641.0356617100
	0.6653700000	−1641.0399894200
	0.7762700000	−1641.0446962900
	0.8871600000	−1641.0495144900
	0.9980200000	−1641.0541594800
	1.1088100000	−1641.0583919400
	1.2195400000	−1641.0620744200
	1.3302400000	−1641.0651987300
	1.4409500000	−1641.0678267300
	1.5516600000	−1641.0700377400
	1.6623500000	−1641.0719128200
	1.7730600000	−1641.0735279300
	1.8838200000	−1641.0749458900
	1.9946200000	−1641.0762096100
	2.1054500000	−1641.0773451200
	2.2162900000	−1641.0783690000